Meat and Muscle Biology™

Categorization of Beef *Longissimus Lumborum* and *Gluteus Medius* Muscles Based on Metabolic Attributes Is More Informative Than Muscle pH

D. Andy King*, Steven D. Shackelford, Dan Nonneman, Tatum S. Katz, and Tommy L. Wheeler

USDA–ARS, Roman L. Hruska US Meat Animal Research Center, Clay Center, NE 68933, USA
*Corresponding author. Email: andy.king@usda.gov (D. Andy King)

Abstract: Muscle metabolism is generally monitored using muscle pH. However, pH does not account for all metabolic effects on meat quality. We evaluated the effectiveness of agglomerative hierarchical clustering in creating clusters of beef *longissimus* and *gluteus medius* muscles based on metabolic traits. Beef carcasses ($n = 100$) were selected at grading based on *longissimus* thoracis pH (<5.6, 5.60 to 5.74, 5.75 to 5.9, and >5.9). Metabolic traits characterizing oxidative and glycolytic metabolism were measured on each muscle. A subset of *longissimus lumborum* muscles were placed in an *in vitro* glycolytic system with 2 temperature decline rates to evaluate glycolytic efficiency. *Gluteus medius* muscles exhibited more oxidative metabolism than *longissimus lumborum* muscles. Metabolic traits measured in one muscle were generally positively correlated to the same trait measured in the other muscle. Clustering of metabolic traits within each muscle produced similar dendrograms. Clustering of *longissimus lumborum* muscles based on metabolic traits produced 4 distinct clusters (High pH, Glycolytic, Chaperone, and Soluble). Clustering of the high pH was generally, but not totally, in agreement with classifications based on pH. The remaining *longissimus lumborum* clusters did not differ in pH. Similar to the *longissimus lumborum* clusters, the *gluteus medius* clusters included High pH and Glycolytic clusters and a cluster with low values for protein solubility and peroxiredoxin 2 abundance. In the *in vitro* system, pH decline was affected by a cluster × temperature decline rate interaction ($P < 0.05$). The soluble cluster had the least extensive pH decline under the fast temperature decline but had the most rapid pH decline at the slower pH decline. These results indicate that clustering muscles based on several metabolic factors was more effective than categorizing muscles based on muscle pH. Metabolic variation identified by clustering was related to differences in the glycolytic machinery that can be differentially impacted by chilling rate.

Keywords: beef, *gluteus medius*, *longissimus lumborum*, metabolism, pH
Meat and Muscle Biology 9(1): 18388, 1–20 (2025) **doi:10.22175/mmb.18388**
Submitted 28 September 2024 Accepted 12 December 2024

Introduction

Muscle metabolism has a profound effect on meat quality. Often, muscle pH is used as the primary indicator of muscle metabolism. Previous research has examined the complex relationship between muscle metabolism and the resulting pH decline (England et al., 2016; Scheffler, 2024; Wang et al., 2024).

Postmortem glycolysis, driven by the breakdown of glycogen, is a primary driver of pH decline in muscle. Most attention has been focused on the accumulation of lactate as a result of anaerobic, glycolytic metabolism (England et al., 2016, England et al., 2014, Rhoades et al., 2005). Thus, the rate and extent of postmortem pH decline on various meat quality attributes has been a significant focus of research (Eilers et al., 1996; Jeremiah et al., 1991; Jones and Tatum, 1994).

While the influence of glycolytic metabolism on pH decline is well-established, it is only one of many energy-producing pathways functioning in skeletal muscle, and the muscle is able to adjust to various conditions. Flux through these pathways may moderate postmortem pH decline and may have direct effects on meat quality traits independent of muscle

pH. In particular, mitochondrial activity can delay pH decline (Ramos et al., 2020; Scheffler et al., 2015). Moreover, mitochondrial processes have direct effects on tenderness (Ramos et al., 2020; Scheffler, 2024; Wright et al., 2018) and color stability (Mitacek et al., 2019; Ramanathan et al., 2020; Ramanathan et al., 2019).

Previous work from our laboratory found that agglomerative hierarchical clustering of beef *longissimus* muscles based on several metabolic traits created groupings that were generally but not entirely consistent with segmentation based strictly on muscle pH (King et al., 2024). Specifically, some muscles that had normal pH were classified as dark cutting muscles. Thus, it is apparent that muscle pH alone does not completely characterize the metabolic status of the muscle.

It is possible that functional variation in the glycolytic machinery contributes to animal-to-animal differences in other metabolic traits. Scopes (1974) developed an *in vitro* model that assesses the function of the glycolytic system in muscle samples. This model has been used to characterize metabolic differences in muscles (Apaoblaza et al., 2020; Scheffler et al., 2015).

The objectives of the present study were to contrast metabolic traits of beef *longissimus lumborum* and *gluteus medius* muscles, evaluate the degree of correlation of metabolic traits in *longissimus lumborum* traits to those in *gluteus medius* muscles, use agglomerative hierarchical clustering to segment both muscles based on biochemical traits, excluding muscle pH, and contrast those groupings to assess relationships among metabolic traits in each muscle. An additional objective was to compare the function of the glycolytic machinery across clusters in *longissimus lumborum* muscles.

Materials and Methods

This study utilized subprimals obtained from chilled carcasses at a USDA Food Safety and Inspection Service (FSIS)–inspected processing facility. As the research involved no live animal handling or interventions, animal care and use committee review was not required.

Experiment 1

Sample handling and preparation. As they were presented for grading at approximately 24 h postmortem, commodity USDA Choice and Select grade beef carcasses ($n = 100$) were screened for inclusion in this study. Muscle pH was measured on the posterior aspect of the *longissimus thoracis* exposed by ribbing the carcass at the 12th to 13th rib interface (loin eye). Carcasses were selected to have *longissimus* thoracis pH less than 5.6, 5.60 to 5.74, 5.75 to 5.9, and greater than 5.9 ($n = 25$ from each group). Measurements of muscle pH were made simultaneously with 2 identical pH probes (FC 200 B series electrode, Hanna Instruments, Woonsocket, RI) attached to identical REED SD-230 pH meters (Reed Instruments, Wilmington, NC). For a carcass to be included in the study, both measurements were required to be in the same category. Strip loins, similar to IMPS #180 (USDA, 2014), and top sirloin butt, similar to IMPS #184 (USDA, 2014), were obtained from the left side of each carcass after fabrication and transported to the US Meat Animal Research Center. A muscle sample (approximately 50 g) was removed from the most anterior aspect of the *longissimus lumborum* and *gluteus medius* muscles for laboratory muscle pH determination at approximately 48 h postmortem. Subprimals then were vacuum packaged and stored at 4°C until 14 d postmortem.

After aging, subprimals were unpackaged. Strip loins were trimmed free of subcutaneous fat, and the *multifidous dorsi* was removed. The remaining *longissimus thoracis et lumborum* muscle was cut into 28-mm-thick steaks with a Graselli NSL400 slicer (Grasselli-SSI, Throop, PA). Steaks 1, 2, 3, and 5 were used in concomitant experiment. Steak 4 was used to measure oxygen consumption and nitric oxide metmyoglobin reducing ability, and the remainder was pulverized for use in other laboratory analyses. The top sirloin butt was trimmed to isolate the *gluteus medius* (with the *gluteus accessorius* removed; similar to IMPS #184B (USDA, 2014)). *Gluteus medius* muscles were cut into 28-mm-thick steaks with the Graselli NSL400 slicer (Grasselli-SSI, Throop, PA). Steaks 1, 3, and 4 were reserved for concurrent experiments. Steak 2 was pulverized in liquid nitrogen and used for laboratory analyses.

pH, myoglobin concentration, and 2-thiobarbituric acid reactive substances (TBARS) determination. Muscle pH was determined on samples obtained at 48 h postmortem using the iodoacetate method of Bendall (1973) with a Reed SD-230 handheld pH meter with a pH probe (Omega PHE 2385 pH probe, Omega Engineering Inc., Stamford, CT). The pH meter was calibrated with standardized pH solutions (pH 4 and pH 7) at approximately 10-sample intervals.

Myoglobin concentration was determined on samples aged for 14 d using a modification of the method reported by Hunt and Hedrick (1977) with additional washing of the pellet (2 times) as described by McKeith et al. (2016) to ensure complete pigment

extraction. Absorbance spectra at 525 nm and 700 nm were collected using a Spectramax plus 96-well plate reader (Molecular Devices, Sunnydale CA). Myoglobin concentration (mg/g meat) was calculated using Beer's law after taking the difference between the absorbance at 525 nm and 700 nm, a millimolar extinction coefficient of 7.6 mM^{-1} cm^{-1}, the molecular weight of myoglobin (17,000 Da), and the appropriate dilution factor.

Quantification of 2-thiobarbituric acid reactive substances (TBARS) was conducted on 14-d aged samples using a Quantichrom TBARS Assay Kit (DTBA-100; Fisher Scientific). One g of pulverized muscle tissue was homogenized with 2 ml of 10% tricarboxylic acid (TCA) and incubated under refrigeration (2°C) for 5 min before centrifugation at 30,000 × g for 15 min at 4 °C. Supernatant (200 µl) was added to 200 µl TBA Reagent and incubated at 100°C for 60 min. Samples were cooled to room temperature before 100 µl of each sample was plated in triplicate into a 96-well plate and read at 535 nm. Concentration of TBARS was calculated using a standard curve (0 to 30 µM malonaldehyde).

Oxygen consumption and nitric oxide metmyoglobin reducing ability. A cube (2.54 cm × 2.54 cm × steak thickness) was removed from each steak. The surface portion was separated from the interior via a horizontal cut through the center of the steak thickness dimension. The top portion (previous steak surface) was used for nitric oxide metmyoglobin reducing ability. The remaining portion (previous steak interior) was used for oxygen consumption measurement.

As described by McKeith et al. (2016), oxygen consumption was measured as the proportion of surface myoglobin in the oxygenated formed after incubation in atmospheric conditions (Bloom). Samples were covered with polyvinyl chloride film [stretchable meat film 55003815; Prime Source, St. Louis, MO; oxygen transmission rate of 1.4 mL/(cm2·24 h) at 23°C] and incubated in air at 4°C for 2 h. Spectral reflectance was scanned with a Hunter Miniscan EZ (HunterLab, Reston, VA) with a 10° observer and 25 mm port immediately after vacuum packaging. The proportion of oxymyoglobin was calculated using equations in King et al. (2023).

Reducing capacity was estimated by measuring the initial levels of metmyoglobin formed after incubation with 0.03% sodium nitrite for 30 min at 20°C. After incubation, samples were blotted, and the proportion of surface metmyoglobin was immediately determined with a colorimeter as previously described. Surface metmyoglobin was calculated using the equations prescribed by King et al. (2023).

Glycolytic potential and glycolytic metabolites. Metabolite concentrations were determined using coupled enzyme assay systems described by Bergmeyer (1974) adapted for use with 96-well plates and using standard curves as described by Hammelman et al. (2003) with additional modifications. One gram of powdered tissue was deproteinated by homogenization with 4 volumes of 2 M hydrochloric acid. One milliliter of homogenate was immediately removed for digestion with amyloglucosidase (AGS) for residual glycogen determination. The remaining homogenate was centrifuged at 30,000 × g for 20 min at 4°C. Supernatant was neutralized with approximately 650 µl of 5.4 M potassium hydroxide to a pH of approximately 7.0. Neutralized samples were stored in refrigeration until use for glucose, glucose-6-phosphate, lactate, and malate assays.

To quantify glycogen, a 200 µl aliquot of homogenate was added to 1 ml of amyloglucosidase (AGS; 10 mg/ml) in 0.2 M acetate buffer and 50 µl of 5.4M potassium chloride and incubated for 3 h at 37°C (pH = 4.8). Digestion was halted with 100 µl of 2M hydrochloric acid and neutralized with 40 µl of 5.4 M potassium chloride. Samples were centrifuged at 30,000 × g for 20 min at 4°C. A 400 µl aliquot of supernatant was added to a glass test tube containing 0.3 M triethanolamine, 1 mM adenosine triphosphate (ATP), 0.9 mM nicotinamide adenine diphosphate (NADP), 4.0 mM $MgSO_4$ with a total volume of 2.3 ml. Absorbance (340 nm) of aliquots (210 µl) in a 96-well plate was read at 340 nm on a Spectramax plus 96-well plate reader (Molecular Devices, Sunnydale, CA, USA). Glucose-6-phosphate dehydrogenase (4 IU) and hexokinase (2 IU) in 80 µl of 3.2 M ammonium sulfate were added to each tube. Tubes were vortexed and incubated at room temperature for 20 min. After incubation, absorbance (340 nm) was determined on triplicate aliquots (210 µl). The increase in absorbance was compared to a standard curve of (0 to 1 mmol glucose) subjected to the same reaction. Glucose and glucose-6-phosphate concentrations from assays of undigested samples (described below) were subtracted from overall glycogen content to determine the final glycogen content.

For glucose and glucose-6-phosphate determination, the same reaction conditions were used on deproteinated, non-digested samples as those described for glycogen determination with the exception that glucose-6-phosphate dehydrogenase and hexokinase were added in separate steps with 20 min incubations at 20°C after each addition. Aliquots (210 µl) were plated before the reaction and after each incubation step,

and absorbance at 340 nm was obtained. Glucose-6-phosphate was calculated using the increase in absorbance during the first incubation, and glucose was determined with the absorbance increase during the second incubation as described above.

To determine lactate, 10 µl extracted and neutralized sample was combined with 190 µl of 1.71 M HCl, 661 mM KOH, and then added an assay system containing 0.43M glycine, 0.34 M hydrazine, 2.74 mM nicotinamide adenine dinucleotide (NAD) with a pH of 9.0 and a total volume of 3.4 ml. Absorbance was read at 340 nm on Spectramax plus 96-well plate reader (Molecular Devices, Sunnydale, CA, USA). Twenty IU lactate dehydrogenase (in 40 µl of 0.4 M hydrazine, 0.5 M glycine; pH 9.0) was added into each sample tube, and tubes were incubated (25°C) for 2 h. Absorbance was again measured (340 nm). The increase in absorbance was compared to the increases observed in a standard curve (0 to 2 mmol) subjected to the same reaction system. Glycolytic potential was reported as the total of lactate equivalents present in the muscle (Monin and Sellier, 1985), where $GP = 2[(\text{glycogen}) + (\text{glucose}) + (\text{glucose-6-phosphate})] + [\text{lactate}]$.

Malate was assayed by adding a 200 µl aliquot of extracted and neutralized sample to an assay system containing 0.43 M glycine, 0.34 M hydrazine, 2.6 mM NAD (pH = 9.0) and a total volume of 3.6 m. Absorbance was read at 340 nm on a Spectramax plus 96-well plate reader (Molecular Devices, Sunnydale, CA, USA). Malate dehydrogenase (80 IU in 40 µl of 0.4M hydrazine, 0.5M glycine; pH 9.0) was added to each reaction. Reactions were incubated at 25°C for 2 h. Absorbance was read again at 340 nm. Malate was calculated using the increase in absorbance compared to a standard curves (0 to 600 µmol malate) in the same reaction system.

Mitochondrial DNA copy number. Relative mitochondrial abundance was assessed as the total number of copies of mitochondrial DNA present in the muscle relative to the nuclear DNA present in the muscle.

Extraction of DNA was performed using the Promega Wizard SV 96 Genomic DNA Purification System (Promega Corp, Madison, WI) following the manufacturer's instructions, ensuring complete digestion of the muscle sample before isolating DNA. DNA (40 ng) was added to wells in a 384-well plate (Bio-RAD Hard Shell 384-23ll Green Plates, Hercules, CA). Six wells were loaded with each DNA sample for triplicate mitochondrial and nuclear amplification. Plates were dried after addition of DNA. Mitochondrial and nuclear DNA was amplified by real-time RT-PCR using primers for NADH dehydrogenase 1 (ND1; forward primer ND1-3278F ccactacgacccgctacatc and reverse primer ND1-3438R, acggctaggcttgatatggc), and nuclear DNA was quantified using primers for vitamin D binding protein, group specific component (GC; forward primer GC-24746F, acctccttgatgcagtcctc, and reverse primer, GC-24686R, caaatttgcccagaaagtgc) in separate reactions. The amplicons were 161 and 120 bp for ND1 and GC, respectively. To each well, 4.5 µL of water, 5 µL of EvaGreen Supermix containing (Bio-Rad catalog #170- 8893), and 0.25 µL each primer (10 µM, 0.25 µM final) in a 10 µL reaction. Initial denaturation was for 3 min at 98°C followed by 39 cycles of 10 s at 98°C and 30 s at 57°C each. A melting curve was performed at 65°C to 95°C at 5 s per step. Copy number of mitochondrial DNA was calculated as described by Schmittgen and Livak (2008) using the equation: $2 \times 2^{\Delta Ct}$, where ΔCt = average nucDNA CT − average mtDNA CT (CT; cycle threshold).

Heat shock protein 70 and peroxiredoxin 2 abundance. For heat shock protein 70, muscle (1 g ± 0.05) was homogenized in 25 ml phosphate buffered saline (PBS; 137 mM sodium chloride, 2.7 mM potassium chloride, 10 mM sodium phosphate, 1.8 mM potassium phosphate; pH = 7.4) and then held (−20°C) for 10 min. Samples were mixed and held (−20°C) for an additional 10 min before centrifugation (15,000 × g; 15 min; 4°C). Supernatant was used for heat shock protein 70 quantification using a Bovine Heat Shock Protein 70 ELISA kit (Catalog number MBS736940; My BioSource.com, San Diego, CA) using reagents and instructions provided by the manufacturer.

For peroxiredoxin 2, muscle tissue (1 g ± 0.05) was homogenized in 25 ml phosphate buffered saline (PBS; 137 mM sodium chloride, 2.7 mM potassium chloride, 10 mM sodium phosphate, 1.8 mM potassium phosphate; pH = 7.4) and then held (−20°C) overnight. Samples were thawed and centrifuged (20,000 × g; 15 min; 4°C). Supernatant was used for peroxiredoxin 2 quantification using a Bovine Peroxiredoxin 2 ELISA Kit (Catalog No: MBS2883044 Sandwich, MyBioSource.com, San Diego, CA) using reagents and instructions provided by the manufacturer.

Carbonyls in soluble, insoluble, and mitochondrial fractions. Extraction and quantification of soluble and insoluble fractions along was completed using methods provided in Rowe et al. (2004). The mitochondrial fraction was isolated and mitochondrial protein concentration determined according to

Cawthon et al. (2001) and Iqbal et al. (2005) as modified by McKeith et al. (2016). Carbonyls on proteins from each fraction were determined by incubation with 2,4-dinitrophenylhydrazine (DNPH) to quantify the extent of oxidative damage in each muscle fraction following the protocol of Reznick and Packer (1994) as modified by Rowe et al. (2004) and McKeith et al. (2016).

Myosin heavy chain isoforms. A whole muscle extract was utilized to quantify the proportion of myosin heavy chain isotypes. One gram of frozen, powdered sample was homogenized in 10 volumes of TRIS-EDTA buffer (tris(hydroxymethyl)aminomethane-ethylenediaminetetraacetic acid) for 20 s using a Polytron at setting #4 (Kinematica Polytron™ PT 2100 Homogenizer, Kinematica, Inc, New York, NY). A 0.5 ml aliquot of homogenized sample was transferred to a 1.5 ml microcentrifuge tube. Then, 0.5 ml of 2x treatment buffer, pH 6.8 (0.125 M Tris, 4% EDTA, 20% glycerol, water) was added to the sample tube, and samples were incubated in a 50°C water bath for 20 min. Mixing was repeated, and samples were reheated for an additional 5 min. Samples were centrifuged for 20 min at 16,000 × g to pellet insoluble material, and protein concentration was determined on the supernatant using Pierce micro-BCA Protein Assay Kit (Thermo Scientific, Waltham, PA). Samples were diluted to 0.3 mg/ml with 2 × Treatment Buffer, pH 6.8 (0.125 M Tris, 4% EDTA, 20% glycerol; pH = 6.8) containing 5% 2-mercaptoethanol and 0.8% bromophenol blue.

Myosin heavy chain (MHC) isoforms were separated and quantified using methods described in Picard et al. (2011) with modifications. Protein (2.7 µl) was loaded on 9% acrylamide separating gel with 6% acrylamide stacking gels. Upper and lower chamber running buffers were made fresh daily. Upper chamber running buffer contained 5× running buffer (100mM Tris, 150mM glycine) diluted to 1× running buffer with H_2O, 0.1% SDS, and 0.07% 2-mercaptoethanol. Lower chamber running buffer contained 5× running buffer (50 mM Tris, 75 mM glycine) diluted to 1X running buffer with H_2O, and 0.05% SDS. Electrophoresis modules run at 70 V for 30 h (7°C).

Gels were washed 3 times for 5 min with destilled and deionized H_2O and stained with Imperial Protein Stain (Thermo Fisher Scientific, Waltham, MA, USA) 1 h with gentle shaking. Stained gels were washed with dd H_2O, first for 30 min and then overnight with gentle shaking. Gels were imaged using the Bio-Rad GelDoc Go Imaging System (Bio-Rad, Hercules, CA, USA), and gels were analyzed using Image Lab Software (Version 6.1, Bio-Rad, Hercules, CA, USA) to determine percent myosin heavy chain type of samples. Samples were analyzed in duplicate, and values were averaged to determine value (%) of MHC-1 (type I fibers) and MHC-2 (type II fibers) in each sample. The differing isoforms of type II MHC did not adequately separate to quantify individually. Thus, only the percentage of type I fibers are reported.

Experiment 2

Longissimus lumborum samples were randomly selected from each of the pH categories on which carcass selection was based ($n = 12$ from each pH category). From each muscle, pulverized tissue (2 g ± 0.05) was placed in an *in vitro* system described by Scopes (1974) and modified by Apaoblaza et al. (2020) with further modification. Duplicate samples from each muscle were homogenized in 20 ml of anaerobic reaction buffer (10 mM sodium phosphate, 5 mM magnesium chloride, 60 mM potassium chloride, 5 mM ATP, 0.5 mM ADP, 0.5 mM NAD, 25 mM carnosine, 30 mM creatine, 10 mM sodium acetate, 50 mM glycogen). System pH was adjusted to 7.0, and samples were placed into water baths heated to 30°C in a refrigerated room (7°C). Two different water baths were used to mimic two different temperature declines (Figure 1). The water bath designated to mimic the fast temperature was turned off with the lid closed at the beginning of the trial and allowed to equilibrate to ambient temperatures (7°C). The temperature setting of the water bath designated to mimic a slow temperature decline was lowered by 1°C each hour for 8 h and then turned off. Aliquots (1 ml) were removed from each homogenate and mixed with 100 µl of 2M hydrochloric acid at 0, 3, 6, and 24 h of incubation. At each of these time points, sample pH was also measured with Reed SD-230 handheld pH meter with a pH probe (Omega PHE 2385 pH probe, Omega

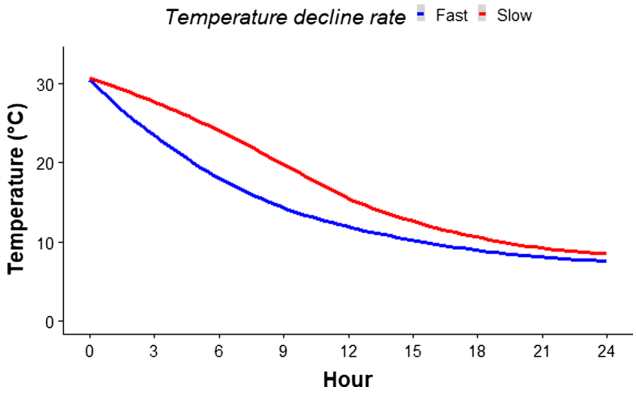

Figure 1. Temperature decline curves for Fast and Slow temperature decline treatments in an *in vitro* system.

Engineering INC., Stamford, CT) calibrated with a three-point (4.0, 7.0, and 10.0) set of standards.

Aliquots removed from the *in vitro* system allowed to rest under refrigeration (4°C) for 15 min and then were centrifuged (16,000 × g) for 18 min at 8°C. Supernatant was neutralized with 10 µl 5.4 M potassium hydroxide for metabolite analyses. Glucose, glucose-6-phosphate, and lactate were determined on each aliquot using the previously described coupled enzyme assay systems.

Statistical analysis

Experiment 1. Within each muscle, relationships among metabolic traits, excluding muscle pH, were assessed using the PCA() function from the FactoMineR package (Le et al., 2008) for R (R Development Core Team, 2008). The PCA analysis (first 5 components) were used to derive the distance matrix for agglomerative hierarchical clustering using the HCPC() function from the Facto Mine R package (Le et al., 2008).

For muscle comparisons, data were analyzed as a randomized complete block using the PROC GLIMMIX procedure of SAS (version 9.4, Cary, NC). The model included the fixed effect of muscle and carcass as the block. The Kenward-Rogers degrees of freedom approximation was used for each model. For comparisons of cluster groupings, data were analyzed as a completely randomized design with the fixed effect of cluster with the PROC GLIMMIX procedure with the Kenward-Rogers degrees of freedom approximation. A P value of 0.05 was used for judgements of statistical significance.

Pearson correlation coefficients were generated for all of the measured metabolic traits in the *longissimus lumborum* muscles to the same groups of traits in the *gluteus medius* using the rcorr() function in the Hmisc package (Harrel et al., 2020) in R. In addition, the traits themselves were clustered within each muscle. The Euclidian distance matrix among scaled metabolic traits within each muscle was generated with the get_dist() function in the factoextra package (Kassambara and Mundt, 2020) and clustered using the hclust() function in base R using Ward's method. The clusters were visualized using the as.dendrogram() function in base R. A tanglegram was generated to compare the alignment of the dendrograms derived from the different muscles using the tanglegram() function from the dendextend package (Galili, 2015).

Experiment 2. Metabolite and pH data from the *in vitro* system were analyzed as a completely randomized design with repeated measures using the PROC GLIMMIX of SAS. The model included the fixed effects of cluster, temperature decline rate, hour, and all possible interactions. The ddfm = kr option was used on the model statement. Hour was the random term and carcass was the subject for the repeated measures, and an autoregressive covariance structure was used. Least-squares means were generated for significant interactions. A P value of 0.05 was used for judgements of statistical significance. Additionally, the rate of pH decline in the *in vitro* system was estimated using an exponential decay function: $pH_t = (pH_0 - pH_f)^{-\alpha t}$, where pHt is the system pH at time t, pH_0 is the system pH at time 0, pH_f is the final system pH value, and t is the time of incubation in hours. For each cluster and temperature decline rate combination, the system pH decline data were fit and the rate (α) were calculated using the nls() function of base R.

Results and Discussion

Experiment 1: Muscle differences in metabolic traits and clustering of longissimus lumborum and gluteus medius muscles based on metabolic traits

As expected, *longissimus lumborum* and *gluteus medius* muscle differed considerably in metabolic characteristics. Least-squares means for comparisons of metabolic traits across muscles in the present study are presented in Table 1. *Longissimus lumborum* muscles had higher ($P < 0.001$) muscle pH at 48 h than *gluteus medius* muscles. *Gluteus medius* muscles had greater ($P < 0.001$) glycolytic potential and higher concentrations ($P \leq 0.02$) of glycogen, glucose, and glucose-6-phosphate compared to *longissimus lumborum* muscles. *Longissimus lumborum* had greater ($P = 0.02$) proportion of type I muscle fibers, although the magnitude of this difference was very small. *Gluteus medius* muscles had greater levels of myoglobin ($P < 0.001$).

Longissimus lumborum muscles had a much greater ($P < 0.001$) abundance of peroxiredoxin 2, and *gluteus medius* had a greater ($P < 0.001$) abundance of heat shock protein 70. *Longissimus lumborum* muscles had greater ($P < 0.01$) oxidation of muscle proteins as evidenced by carbonyls on myofibrillar and sarcoplasmic proteins. However, carbonyls on mitochondrial proteins did not differ between *longissimus lumborum* and *gluteus medius* proteins.

Mitochondrial protein abundance was greater ($P <$ 0.001) in *gluteus medius* muscles than in *longissimus*

Table 1. Least-squares means for metabolic traits for beef *longissimus lumborum* and *guteus medius* muscles

	Longissimus lumborum			*Gluteus medius*			
Trait	Mean		SEM	Mean		SEM	$P > F$
pH	5.73	±	0.03	5.58	±	0.03	<0.001
Glycolytic potential, µmol/g	194.12	±	4.79	207.85	±	4.79	<0.001
Glycogen, µmol/g	9.07	±	1.02	10.66	±	1.02	0.02
Glucose, µmol/g	5.02	±	0.33	6.75	±	0.33	<0.001
Glucose-6-phosphate, µmol/g	5.42	±	0.39	6.14	±	0.39	<0.01
Lactate, µmol/g	155.11	±	2.65	160.75	±	2.65	0.06
Malate, µmol/g	0.41	±	0.04	0.37	±	0.04	0.23
Type I fibers, %	34.98	±	0.27	34.39	±	0.27	0.02
Mitochondrial copy number	1716.15	±	97.47	1917.07	±	97.47	0.15
Myoglobin, mg/g	4.35	±	0.09	5.62	±	0.09	<0.001
Peroxiredoxin 2, ng/g	404.70	±	11.72	261.45	±	11.72	<0.001
Heat shock protein 70, ng/g	4.82	±	0.23	6.42	±	0.23	<0.001
TBARS, µmol MDA/g	11.46	±	0.71	12.20	±	0.71	0.11
Protein solubility, %	11.18	±	0.22	11.09	±	0.22	0.56
Myofibrillar carbonyls, µmol/mg	5.87	±	0.34	4.61	±	0.34	0.01
Sarcoplasmic carbonyls, µmol/mg	1.68	±	0.10	1.41	±	0.10	0.02
Mitochondrial carbonyls, µmol/mg	7.66	±	0.38	7.81	±	0.38	0.68
Mitochondrial protein, mg/g	0.39	±	0.02	0.48	±	0.02	<0.001
Initial metmyoglobin formation[1], %	59.43	±	0.50	62.78	±	0.50	<0.001
Bloom[2], %	69.70	±	0.90	78.20	±	0.90	<0.001

[1]Initial metmyoglobin formation = percentage of surface myoglobin in the metmyoglobin form after incubation with 0.3% sodium nitrite.

[2]Bloom = percentage of surface myoglobin in the oxymyoglobin form after incubation with atmospheric oxygen.

lumborum muscles. However, this coincides with lesser ability to reduce metmyoglobin after incubation with 0.03% sodium nitrite and greater oxygenation of myoglobin during exposure to atmospheric oxygen ($P <$ 0.001; initial metmyoglobin formation and bloom, respectively). We speculate that these results are a function of lesser functionality of mitochondrial processes in *gluteus medius* muscles. However, this difference in apparent mitochondrial functionality may be due to muscle pH. The *gluteus medius* has previously been reported to have greater oxygen consumption and reducing activity than the *longissimus lumborum* (McKenna et al., 2005). However, previous work has demonstrated that *longissimus* muscles with greater muscle pH possessed greater reducing capacity and oxygen consumption than those with lower muscle pH (English et al., 2016; King et al., 2024; McKeith et al., 2016).

To further understand the relationships of the metabolic traits within and across muscles, cluster analysis was conducted on the metabolic variables for each muscle. Moreover, Pearson correlation coefficients were generated to compare the relationships of metabolic traits and clusters of traits between *longissimus lumborum* and *gluteus medius* muscles (Figure 2A). *Longissimus lumborum* metabolic traits were segmented into 4 clusters. The first, LM_1, consisted of protein solubility, carbonyls on sarcoplasmic proteins, and malate concentration. The second cluster, LM_2, was composed of carbonyls on mitochondrial and myofibrillar proteins, and muscle pH. Cluster LM-3 was composed of myoglobin, proportion of muscle fibers with myosin heavy chain type I, abundance of mitochondrial DNA, peroxiredoxin 2 and heat shock protein 70. Glycolytic potential, lactate, bloom, initial metmyoglobin formation, glucose, glucose-6-phosphate, glycogen, abundance of mitochondrial protein, and TBARS made up cluster LM_4.

The make-up of the clusters of metabolic traits from *gluteus medius* muscles was similar to those for *longissimus lumborum*. Cluster GM_1 was composed of protein solubility, abundance of peroxiredoxin 2, and malate concentration. Carbonyls in sarcoplasmic and myofibrillar proteins as well as muscle pH made up cluster GM_2. Myoglobin concentration, carbonyls in mitochondrial proteins, proportion of type I fibers, abundance of mitochondrial DNA and heat shock protein 70 comprised cluster GM-3. Cluster GM-4 included glycolytic metabolism traits, such as glycolytic potential, glucose-6-phosphate, glucose, glycogen, and lactate. Additionally, this cluster included bloom, initial metmyoglobin formation, mitochondrial protein abundance, and TBARS.

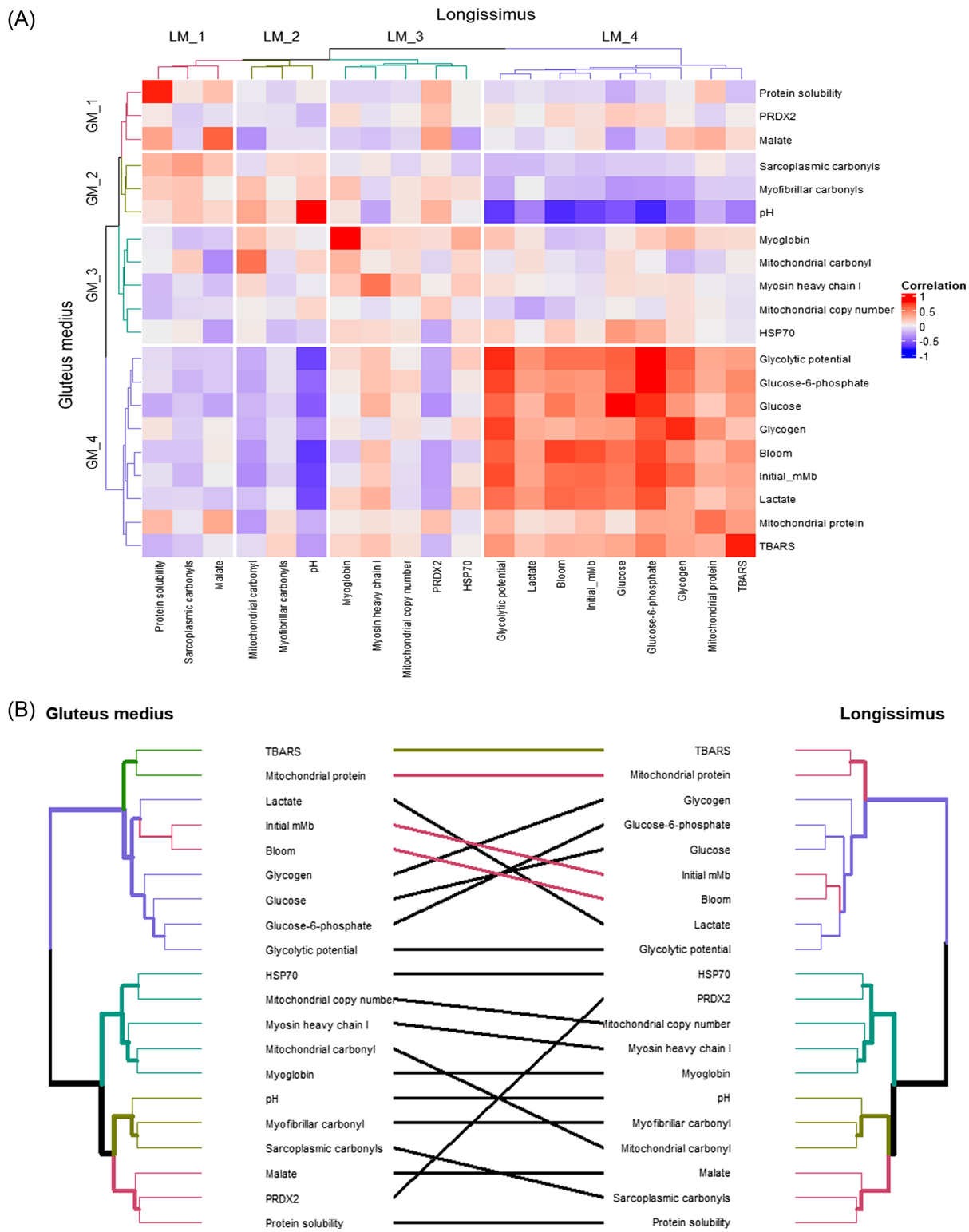

Figure 2. Heatmap of Pearson correlation coefficients of metabolic traits measured in *longissimus lumborum* muscles to the same metabolic traits measured in *gluteus medius* muscles (Panel A). Comparison on clustering of metabolic traits in *longissimus lumborum* muscles to the clustering of the same metabolic traits in *gluteus medius* muscles (Panel B).

The correlations among traits included in clusters LM_4 and GM_4 were generally strongly positive. The traits in GM_4 were generally negatively correlated to the traits in LM_2. This was particularly true for the glycolytic traits in cluster GM_4 to *longissimus lumborum* pH. The same relationships were

detected for traits of cluster LM_4 to the traits in cluster GM_2. Correlations of *longissimus lumborum* protein solubility, muscle pH, and myoglobin concentration were particularly strongly positive to the same traits from the *gluteus medius* muscles.

The tanglegram presented in Figure 2B depicts the agreement of clustering metabolic traits of *longissimus lumborum* muscles to the clustering of the same traits in *gluteus medius* muscles. Generally, the relationships among traits with *longissimus lumborum* traits were consistent with those among the same traits in *gluteus medius* muscles. The traits included in LM_4 and GM_4 were the same, although some differences in alignment existed in the dendrograms within the clusters. The abundance of peroxiredoxin 2 was included in cluster GM_1 along with malate and protein solubility. However, in *longissimus* muscles, peroxiredoxin 2 was in included in cluster LM_3 in close association with heat shock protein 70.

Similarly, the abundance of carbonyls on mitochondrial proteins in *gluteus medius* muscles was clustered in close association with myoglobin concentration in GM_3, but in *longissimus* muscles, the abundance of carbonyls on mitochondrial proteins was closely associated with the abundance of carbonyls on myofibrillar proteins in cluster LM_2. In *gluteus medius* muscles, the abundance of carbonyls on sarcoplasmic proteins was closely related to the abundance of carbonyls on myofibrillar proteins in cluster GM_2. In *longissimus lumborum* muscles, sarcoplasmic protein carbonyl abundance was closely related to protein solubility in cluster LM_1.

The *gluteus medius* is generally reported to possess more oxidative metabolic properties than the *longissimus lumborum*. Most of these reports indicate that the *gluteus medius* exhibits greater proportion of type I fibers and mitochondrial content, resulting in greater oxygen consumption than *longissimus lumborum* muscles (Hunt and Hedrick, 1977; Lanari and Cassens, 1991; McKenna et al., 2005). In partial agreement, the present study indicated that *gluteus medius* had greater abundance of mitochondrial protein, greater myoglobin concentration, and greater oxygen consumption, and tended ($P = 0.15$) to have greater copy number of the mitochondrial genome. However, the present study also detected a lesser proportion of type I fibers in *gluteus medius* muscles relative to *longissimus lumborum* muscles although the magnitude of this difference is very small. In contrast, the *gluteus medius* muscles in the present experiment had greater glycolytic potential and greater abundance of the associated metabolites than *longissimus lumborum* muscles. These results may be somewhat skewed by the range of muscle pH values selected for inclusion in the present study. However, these results indicate that while *gluteus medius* may tend to possess more oxidative properties, it also has significant glycolytic capacity relative to *longissimus lumborum* muscles. Metabolic traits were generally positively correlated to the same trait in the other muscle. Clustering of metabolic traits revealed a high degree of similarity in the relationships among metabolic traits across muscles.

Clustering of longissimus muscles based on metabolic traits

Results of the principal component analysis of metabolic traits of *longissimus lumborum* muscles is shown in Figure 3A. Muscle pH was not included in the principal component analysis to enable understanding of relationships among metabolic traits without the influence of a large range of pH values. Component 1

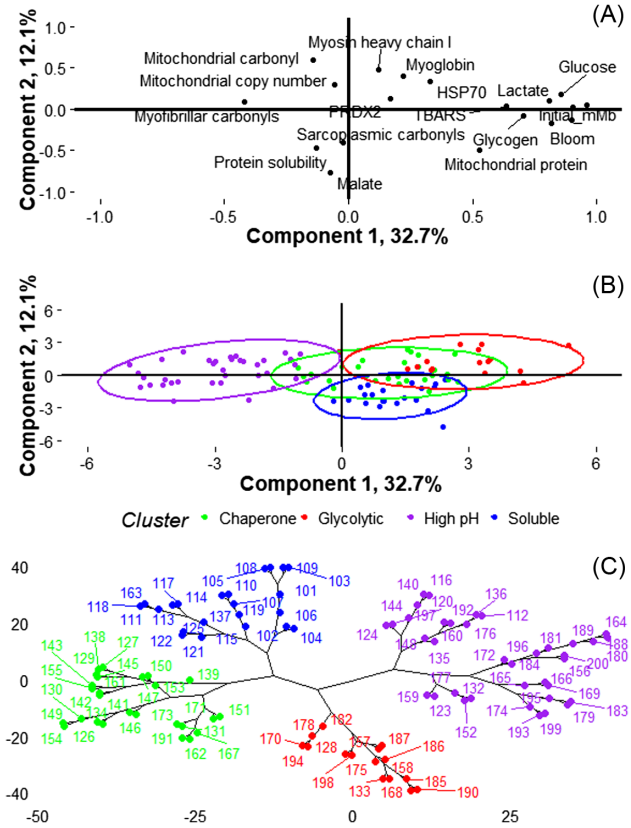

Figure 3. Results of principal component analysis and cluster analysis of metabolic traits in *longissimus lumborum* muscles. Panel A depicts loadings of metabolic traits measured in *longissimus lumborum* muscles. Panel B depicts sample scores of *longissimus* muscles segmented into clusters based on metabolic traits in in PCA analysis. Panel C depicts a phylogenetic tree based on metabolic traits used to cluster *longissimus lumborum* muscles.

explained 32.7% of the variation in metabolic traits of *longissimus lumborum*. Positive loadings for this component were associated with increased initial metmyoglobin formation, bloom, glucose, lactate glycogen, mitochondrial protein, and TBARS. Negative loadings for Component 1 were associated with carbonyls on myofibrillar proteins. Despite leaving muscle pH out of the principal component analysis, it is apparent that Component 1 is highly related to variables that are strongly influenced by muscle pH. Component 2 explained 12.1% of the variation in metabolic traits of *longissimus* muscles. Positive loadings were associated with increased abundance of carbonyls on mitochondrial proteins, proportion of type I fibers, and myoglobin concentration, while negative loadings for Component 2 were associated with increased concentration of malate and protein solubility.

The first 5 components generated by the principal component analysis were used to derive the distance matrix for agglomerative hierarchical clustering. The score plot in Figure 3B show the results of the clustering. The high pH cluster was characterized by negative loadings for Component 1. The glycolytic cluster was associated by positive values for Component 1. The chaperone and soluble clusters were intermediate to the high pH and glycolytic clusters regarding Component 1. The soluble cluster generally had lower values for Component 2 than the chaperone cluster. The phylogenetic tree in Figure 3C depicts the relatedness of the muscles with regard to metabolic factors. It was evident that the clustering analysis resulted in 4 distinct groups of samples to compare metabolic factors.

Agglomerative hierarchical clustering segmented *longissimus lumborum* muscles using metabolic traits, excluding muscle pH. The distribution of *longissimus lumborum* muscles across clusters in comparison to classifications based on muscle pH is presented in Table 2. To aid in interpretation, clusters were given names based on the detected differences in metabolic traits (presented below). All the *longissimus lumborum* muscles with muscle pH greater than 5.90 were included in the High pH cluster. However, 12 individuals with muscle pH between 5.71 and 5.90 and 3 individuals with muscle pH between 5.61 and 5.70 were also included in the High pH cluster. This indicates that some muscles with muscle pH that would be considered normal are more metabolically similar to muscles that would be considered dark cutters. The carcasses with muscle pH between 5.71 and 5.90 would be considered atypical dark cutters (Kirkpatrick et al., 2023). Those investigators reported that metabolism was more oxidative in atypical dark cutters than normal muscle and that dark cutters were even more oxidative. Most of those muscles were included in the High pH cluster, but 8 individuals in this pH category were segmented into other clusters. The *longissimus* muscles with muscle pH values less than 5.6 were distributed into the Chaperone, Glycolytic, and Soluble clusters. The same was true for muscles with pH values between 5.61 and 5.70.

Table 2. Distribution of *longissimus* muscle samples in pH categories and clusters based on metabolic data

pH class	Chaperone	Glycolytic	High pH	Soluble	Total
<5.6	14	12	0	6	32
5.61 to 5.70	7	4	3	14	28
5.71 to 5.90	7	0	12	1	20
>5.90	0	0	20	0	20
Total	28	16	36	21	100

Least-squares means for metabolic traits of *longissimus lumborum* muscles stratified by clustering of metabolic traits are presented in Table 3. The High pH cluster was characterized by the highest ($P < 0.05$) values for muscle pH, which did not differ across the remaining clusters. This coincided with the lowest ($P < 0.05$) concentrations of glycogen, glucose, glucose-6-phosphate, and lactate and consequently the lowest ($P < 0.05$) glycolytic potential. The High pH cluster also had the lowest ($P < 0.05$) abundance of TBARS and mitochondrial protein. The High pH cluster also had the highest abundance of carbonyls on myofibrillar proteins and had greater ($P < 0.05$) abundance of carbonyls on mitochondrial proteins than muscles in the Soluble and Chaperone clusters.

Muscles in the Glycolytic cluster had the highest ($P < 0.05$) glycolytic potential resulting from the highest ($P < 0.05$) muscle concentrations of glycogen, glucose, glucose-6-phosphate, and lactate. Muscles included in the Glycolytic cluster had the lowest ($P < 0.05$) concentration of malate and the highest ($P < 0.05$) myoglobin concentration compared to muscles in the other clusters. Abundance of heat shock protein 70 was higher ($P < 0.05$) in muscles from the glycolytic cluster than in muscles from the High pH and Soluble clusters. Muscles from the Glycolytic cluster had lesser ($P < 0.05$) protein solubility than muscles from the Soluble and High pH clusters. Muscles from the Glycolytic cluster had greater abundance of carbonyls on mitochondrial proteins than muscles in the Chaperone and Soluble clusters. Muscles that were included in the Chaperone cluster had the greatest

Table 3. Least-squares means of metabolic traits of *longissimus lumborum* muscles segmented into clusters based on metabolic traits

	High pH			Chaperone			Soluble			Glycolytic			
Trait	Mean		SEM	Mean		SEM	Mean		SEM	Mean		SEM	$P > F$
pH	6.08[a]	±	0.04	5.57[b]	±	0.04	5.55[b]	±	0.05	5.50[b]	±	0.05	<0.001
Glycolytic potential, µmol/g	137.68[c]	±	4.94	209.42[b]	±	5.52	220.76[b]	±	6.37	255.82[a]	±	7.30	<0.001
Glycogen, µmol/g	1.54[d]	±	1.24	8.26[c]	±	1.39	16.08[b]	±	1.61	17.77[a]	±	1.84	<0.001
Glucose, µmol/g	2.02[d]	±	0.29	7.27[b]	±	0.32	4.20[c]	±	0.37	8.68[a]	±	0.42	<0.001
Glucose-6-phosphate, µmol/g	1.14[c]	±	0.41	6.32[b]	±	0.45	6.92[b]	±	0.52	11.21[a]	±	0.60	<0.001
Lactate, µmol/g	128.26[c]	±	3.64	165.72[b]	±	4.07	166.37[b]	±	4.70	180.51[a]	±	5.38	<0.001
Malate, µmol/g	0.35[b]	±	0.05	0.29[b]	±	0.06	0.95[a]	±	0.06	0.05[c]	±	0.07	<0.001
Type I fibers, %	34.83	±	0.44	35.29	±	0.50	34.27	±	0.57	35.68	±	0.66	0.37
Mitochondrial copy number	1728.07	±	95.01	1701.31	±	106.22	1664.30	±	122.66	1487.85	±	140.52	0.55
Myoglobin, mg/g	4.26[b]	±	0.13	3.95[b]	±	0.15	4.36[b]	±	0.17	5.26[a]	±	0.20	<0.001
Peroxiredoxin 2, ng/g	378.31[b]	±	18.16	465.67[a]	±	20.30	382.97[b]	±	23.44	384.22[b]	±	26.85	<0.01
Heat shock protein 70, ng/g	4.35[b]	±	0.22	5.40[a]	±	0.24	4.12[b]	±	0.28	5.76[a]	±	0.32	<0.001
TBARS, µmol MDA/g	6.42[c]	±	1.02	11.58[b]	±	1.14	13.77[b]	±	1.31	19.22[a]	±	1.50	<0.001
Protein solubility, %	11.48[b]	±	0.35	10.38[c]	±	0.39	12.16[a]	±	0.45	10.63[c]	±	0.52	0.02
Myofibrillar carbonyls, µmol/mg	8.15[a]	±	0.51	2.98[c]	±	0.57	5.32[bc]	±	0.66	6.67[b]	±	0.76	<0.001
Sarcoplasmic carbonyls, µmol/mg	1.61		0.16	1.72		0.18	1.90		0.21	1.49		0.24	0.5911
Mitochondrial carbonyls, µmol/mg	9.40[a]	±	0.54	6.20[b]	±	0.60	4.06[c]	±	0.69	11.12[a]	±	0.79	<0.001
Mitochondrial protein, mg/g	0.30[d]	±	0.02	0.36[c]	±	0.02	0.53[a]	±	0.02	0.45[b]	±	0.02	<0.001
Initial metmyoglobin formation[1], %	52.99[b]	±	0.52	62.21[a]	±	0.58	63.36[a]	±	0.67	63.52[a]	±	0.77	<0.001
Bloom[2], %	59.63[b]	±	0.93	74.80[a]	±	1.04	74.91[a]	±	1.21	75.98[a]	±	1.38	<0.001

[1]Initial metmyoglobin formation = proportion of surface myoglobin in the metmyoglobin state after incubation with 0.03% sodium nitrite.

[2]Bloom = proportion of surface myoglobin in the oxymyoglobin form after incubation in atmospheric oxygen.

[a–d]Least-squares means, within a row, lacking common superscripts differ ($P < 0.05$).

($P < 0.05$) abundance of peroxiredoxin 2 and greater ($P < 0.05$) abundance of heat shock protein 70 than muscles from the High pH and Soluble clusters. Muscles included in the Chaperone cluster had lesser ($P < 0.05$) abundance of carbonyls on myofibrillar proteins than muscles in the Glycolytic and High pH clusters. Muscles included in the Soluble cluster had the greatest ($P < 0.05$) protein solubility and malate concentration compared to muscles in other clusters. In comparison to muscles in the Chaperone cluster, muscles in the soluble cluster had greater ($P < 0.05$) glycogen concentration and mitochondrial protein abundance and lesser ($P < 0.05$) glucose concentration and abundance of carbonyls on mitochondrial proteins.

Clustering of gluteus medius muscles based on metabolic traits

The results of the principal component analysis of metabolic traits, excluding muscle pH, in *gluteus medius* muscles is presented in Figure 4A. Component 1 explained 26.2% of the variation in metabolic traits of *gluteus medius* muscles. Positive loadings for Component 1 was associated with increased glycolytic potential, which coincided with increased concentrations of glucose, glycogen, glucose-6-phosphate, and lactate. Bloom and initial metmyoglobin formation were also associated with positive loadings for Component 1. Negative loadings for Component 1 were associated with increased abundance of peroxiredoxin 2, malate concentration and carbonyls on mitochondrial proteins. As noted for the *longissimus lumborum* muscles, Component 1 was largely related to factors that are highly related to muscle pH. Positive loadings for Component 2 were associated with increased malate concentration and mitochondrial protein. Negative loadings for Component 2 were associated with increased carbonyl abundance on mitochondrial proteins.

The principal component analysis was used to derive the distance matrix for agglomerative hierarchical clustering. The sample score plot in Figure 4B depicts the relationships of the 3 clusters segmenting the *gluteus medius* muscles. The High pH cluster was associated with negative scores for Component 1. The Glycolytic and Low clusters were similar with regard to Component 1, but *gluteus medius* muscles in the Glycolytic cluster generally had higher scores

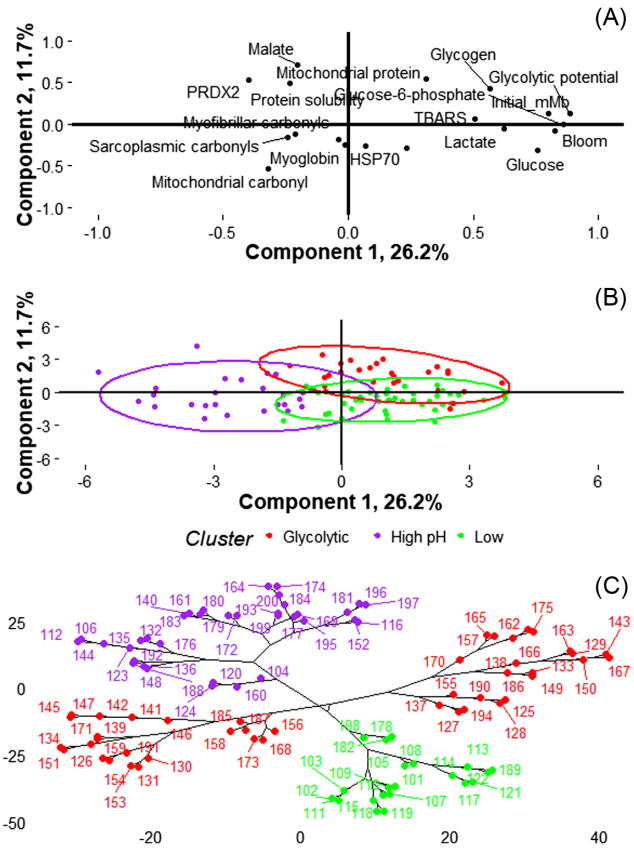

Figure 4. Results of principal component analysis and cluster analysis of metabolic traits in *gluteus medius* muscles. Panel A depicts loadings of metabolic traits measured in *gluteus medius* muscles. Panel B depicts sample scores of *gluteus medius* muscles segmented into clusters based on metabolic traits in in PCA analysis. Panel C depicts a phylogenetic tree based on metabolic traits used to cluster *gluteus medius* muscles.

for Component 2 than muscles from the Low cluster. The phylogenetic tree in Figure 4C indicates that the clustering segmented the *gluteus medius* muscles into 3 distinct groups.

The distributions of *gluteus medius* muscles in the clusters compared to categorization of the muscles based on *longissimus lumborum* pH from the same carcass or from the muscle pH of the *gluteus medius* are shown in Table 4. Twenty carcasses were selected based on *longissimus* muscle pH greater than 5.9. Of these, the *gluteus medius* of 17 were included in the High pH cluster. The remaining 3 were included in the other clusters with muscles from carcasses with normal *longissimus lumborum* values. Categorization of *gluteus medius* muscles based on *gluteus medius* pH did not agree with categorization of *gluteus medius* muscles based on *longissimus lumborum* pH. Of the 100 carcasses included in the study, 76 had gluteus medius pH less than 5.6. Most of those *gluteus medius* muscles were distributed in the Low and Glycolytic clusters.

Table 4. Frequency distribution of *gluteus medius* muscles segmented into clusters based on metabolic data to pH classes based on *longissimus* muscle pH and *gluteus medius* pH

pH Class	Glycolytic	High pH	Low	Total
Gluteus medius clusters compared to longissimus lumborum pH class				
<5.6	7	0	25	32
5.61 to 5.70	16	2	10	28
5.71 to 5.90	2	9	9	20
>5.90	2	17	1	20
Total	27	28	45	100
Gluteus medius clusters compared to gluteus medius pH class				
<5.6	26	6	44	76
5.61 to 5.70	1	7	1	9
5.71 to 5.90	0	7	0	7
>5.90	0	8	0	8
Total	27	28	45	100

Least-squares means for metabolic traits of *gluteus medius* muscles clustered according to metabolic traits are shown in Table 5. Muscle pH was higher ($P < 0.05$) in muscle included in the High pH cluster compared to the other clusters. This coincided with the lowest ($P < 0.05$) glycolytic potential and the lowest ($P < 0.05$) concentrations of glycogen, glucose, glucose-6-phosphate, and lactate relative to the other clusters. Muscles included in the High pH cluster had lower ($P < 0.05$) TBARS than the muscles in the other clusters. However, muscles in the High pH cluster also had greater abundance of carbonyls on mitochondrial proteins compared to muscles in the other 2 clusters. Muscles in the High pH cluster had the lowest values for initial metmyoglobin formation and bloom, indicating that muscles in the High pH cluster had greater ($P < 0.05$) reducing capacity and oxygen consumption, respectively, than muscles from the other clusters.

Gluteus medius muscles included in the Glycolytic cluster had the higher glycolytic potential than muscles in the other clusters. Glycogen, lactate, and malate concentrations were greatest ($P < 0.05$) in muscles included in the Glycolytic cluster compared to muscles in other clusters. Muscles in the Glycolytic cluster also exhibited greater ($P < 0.05$) abundance of mitochondrial protein than muscles included in the other clusters. The Low cluster was so-named because muscles in this cluster had the least ($P < 0.05$) abundance of peroxiredoxin 2 and mitochondrial protein, the lowest ($P < 0.05$) protein solubility, and the lowest ($P < 0.05$) concentration of malate.

In the principal component analyses of both muscles, the component explaining the greatest proportion of variation was associated strongly with

Table 5. Least-squares means of metabolic traits of *gluteus medius* muscles segmented into clusters based on metabolic traits

	High pH			Glycolytic			Low			
Trait	Mean		SEM	Mean		SEM	Mean		SEM	P > F
pH	5.82[a]	±	0.03	5.50[b]	±	0.03	5.49[b]	±	0.02	<0.001
Glycolytic potential, µmol/g	163.80[c]	±	5.91	238.65[a]	±	6.02	216.78[b]	±	4.67	<0.001
Glycogen, µmol/g	3.42[c]	±	1.65	19.58[a]	±	1.68	9.82[b]	±	1.30	<0.001
Glucose, µmol/g	3.50[c]	±	0.44	5.69[b]	±	0.45	9.40[a]	±	0.35	<0.001
Glucose-6-phosphate, µmol/g	1.79[b]	±	0.43	7.84[a]	±	0.44	7.84[a]	±	0.34	<0.001
Lactate, µmol/g	146.39[b]	±	3.99	172.42[a]	±	4.07	162.67[a]	±	3.15	<0.001
Malate, µmol/g	0.37[b]	±	0.05	0.55[a]	±	0.05	0.27[b]	±	0.04	<0.001
Type I fibers, %	33.73[b]	±	0.50	33.58[b]	±	0.51	35.28[a]	±	0.39	0.01
Mitochondrial copy number	2104.39	±	221.28	1912.76	±	225.34	1803.10	±	174.55	0.57
Myoglobin, mg/g	5.72	±	0.18	5.60	±	0.18	5.58	±	0.14	0.82
Peroxiredoxin 2, ng/g	325.66[a]	±	20.11	305.76[a]	±	20.47	194.92[b]	±	15.86	<0.001
Heat shock protein 70, ng/g	6.27	±	0.56	7.46	±	0.57	5.89	±	0.44	0.09
TBARS, µmol MDA/g	7.25[b]	±	1.13	14.19[a]	±	1.15	14.08[a]	±	0.89	<0.001
Protein solubility, %	11.95[a]	±	0.36	12.25[a]	±	0.37	9.87[b]	±	0.28	<0.001
Myofibrillar carbonyls, µmol/mg	4.94	±	0.59	5.02	±	0.60	4.15	±	0.46	0.42
Sarcoplasmic carbonyls, µmol/mg	1.63	±	0.20	1.27	±	0.20	1.36	±	0.16	0.40
Mitochondrial carbonyls, µmol/mg	9.70[a]	±	0.64	6.13[b]	±	0.65	7.64[b]	±	0.51	<0.001
Mitochondrial protein, mg/g	0.40[b]	±	0.03	0.62[a]	±	0.03	0.44[b]	±	0.02	<0.001
Initial metmyoglobin formation[1], %	58.49[b]	±	0.61	65.11[a]	±	0.62	64.05[a]	±	0.48	<0.001
Bloom[2], %	68.42[b]	±	1.18	80.17[a]	±	1.21	83.10[a]	±	0.93	<0.001

[1]Initial metmyoglobin formation = proportion of surface myoglobin in the metmyoglobin state after incubation with 0.03% sodium nitrite.

[2]Bloom = proportion of surface myoglobin in the oxymyoglobin form after incubation in atmospheric oxygen.

[a–c]Least-squares means, within a row, lacking common superscripts differ ($P < 0.05$).

glycolytic capacity, and consequently muscle pH, even though pH was not used in the clustering process. This is not surprising because creating a wide range of muscle pH was a key goal of carcass selection for this study. The second component was generally related to oxidative traits, but many of these traits contributed to both components.

Given this, it is not surprising that, in both muscles, the High pH cluster was the most clearly separated in a biplot of the first two principal components. The remaining clusters, in both muscles, had similar muscle pH. While oxidative metabolic traits differed across these clusters, they were not cleanly separated by Component 2. It is important to note that the first 5 principal components were used in the agglomerative hierarchical clustering. So while Components 3, 4, and 5 explained small proportions of the variation in metabolic traits in these muscles, they did contribute to distance matrix used to differentiate clusters.

In our previous report, we suggested that categorizing muscles based on several metabolic traits would be more effective in understanding the metabolic contributions to meat quality than classification based solely on muscle pH (King et al., 2024). In the present study, categorizing muscles according to agglomerative hierarchical clustering of metabolic traits was generally consistent with muscle pH. Specifically, in *longissimus lumborum* muscles, the high pH class was generally composed of samples that had muscle pH values greater than 5.9, although some muscles with lower pH values were included in that cluster. However, the remaining 3 clusters had similar mean muscle pH values and were composed of samples across pH classes. Thus, differentiating muscles based on metabolic factors would yield more specific results when studying the metabolic contributions to meat quality.

The incidence of dark cutting beef has generally been attributed to the depletion of glycogen stores in response to long-term stress. However, more recently the role of mitochondrial function in predisposing animals to producing dark cutting carcasses has been demonstrated (Kiyimba et al., 2021; McKeith et al., 2016; Ramanathan et al., 2020).

In the present experiment, the High pH cluster of *longissimus lumborum* muscles exhibited low values for glycolytic potential and associated metabolite profiles. This is consistent with the previous reports of observations of glycolytic metabolites in dark cutting

muscles (McKeith et al., 2016; Ramanathan et al., 2020). The results of the present experiment indicate that the High pH muscles had greater abundance of carbonyls on myofibrillar and mitochondrial proteins relative to the other clusters, indicating oxidative damage. McKeith et al. (2016) found that mitochondria from dark cutting muscles lost electrons during electron transport resulting in greater reactive oxygen species compared to normal muscles. Ramanathan et al. (2020) found that dark cutting *longissimus lumborum* muscles had greater mitochondrial protein and a greater copy number of mitochondrial genes than normal muscles. In the present study, mitochondrial protein abundance was lower in the High pH cluster than the other clusters, and mitochondrial copy number did not differ across clusters. The metabolic profile of the High pH cluster for *gluteus medius* was very similar to the one for *longissimus lumborum*, in the present experiment.

The incidence of the dark cutting condition is low (Mayer et al., 2024). So while it is evident that dark cutting beef is associated with a certain metabolic profile, it is not likely that all animals that possess that profile produce dark cutting carcasses. Conversely, it is likely possible for glycogen to be depleted in carcasses not possessing that profile under some conditions.

Commercially, carcasses are generally classified as dark cutters based on lean color, sometimes in conjunction with muscle pH, of the *longissimus* thoracis exposed by ribbing at the 12th and 13th rib interface. Grouping *gluteus medius* muscles according to metabolic traits measured on that muscle yielded much different results than grouping them based on pH of the *longissimus* muscle from the same carcass. Even though 20 of the 100 carcasses included in the present study were selected to have *longissimus lumborum* muscle pH greater than 5.9, only 8 *gluteus medius* muscles had pH this high. The High pH *gluteus medius* cluster included these 8 muscles but also included at least 6 muscles from each pH category. The distribution of muscles into the other two *gluteus medius* clusters was similar across pH classes, indicating that these clusters are representing metabolic variation not characterized by muscle pH.

The Glycolytic cluster for *longissimus lumborum* muscles had the greatest glycolytic potential and all of the glycolytic metabolites measured in the present experiment. This cluster also had the greatest abundance of myoglobin and had more carbonyls on mitochondrial proteins than the soluble and chaperone clusters. Thus, even though samples in the Glycolytic cluster exhibit a high degree of glycolytic capacity, they also exhibit evidence of oxidative function. The glycolytic potential of this cluster was quite high. Previous results from our laboratory indicates that glycolytic potential greater than 130 μmol/g did not result in further decreases in ultimate muscle pH (McKeith et al., 2016), which was consistent with the findings of Wulf et al. (2002). Greater glycolytic capacity is generally reported to be associated with a greater proportion of type II fibers (Ramos et al., 2021). In the present experiment, neither the proportion of type I fibers nor the copy number of mitochondrial DNA differed across clusters. The name of the Chaperone cluster was based on this cluster having the greatest abundance of peroxiredoxin 2 and greater heat shock protein 70 abundance than the High pH and Soluble clusters. Peroxiredoxin 2 functions to scavenge reactive oxygen species and prevents oxidative damage, and greater peroxiredoxin 2 abundance has been associated with less tender meat (Carlson et al., 2017). Johnson et al. (2021) hypothesized that peroxiredoxin 2 increases postmortem in response to oxidative conditions. Heat shock protein 70 functions to stabilize protein and prevent denaturation and aggregation during stressful conditions and has been associated with less tender meat (Picard et al., 2014). The high levels of these chaperone proteins in the muscles from the Chaperone cluster indicate that oxidative or other stress conditions may have occurred during the conversion of muscle to meat. However, relative to the other clusters, indicators of oxidative damage were not particularly high in the muscles included in this cluster. The key feature of the Soluble cluster is the greatest protein solubility relative to the muscles in the other cluster. Muscles in this cluster also had greater mitochondrial protein than muscles from the other clusters. Muscle pH in this cluster was not different from the Chaperone and Glycolytic clusters. Perhaps the increased protein solubility is because these muscles underwent slower pH decline than the muscles in the other cluster.

Experiment 2: In vitro evaluation of glycolytic machinery of longissimus lumborum muscles

The *in vitro* system described by Scopes (1974) was adapted to compare the functionality of the glycolytic machinery in *longissimus lumborum* clusters derived in Experiment 1. Rather than incubate at a constant temperature as prescribed by Scopes (1974), muscle samples in the *in vitro* system were incubated under two temperature profiles to mimic differing carcass chilling rates. Samples were initially selected for this experiment to equally represent original pH classes used for carcass

Table 6. Frequency distribution of *longissimus lumborum* muscles segmented into clusters based on metabolic data to pH classes

pH Class	Chaperone	Glycolytic	High pH	Soluble	Total
<5.6	5	3	0	4	12
5.61–5.70	3	3	3	3	12
5.71–5.90	5	0	6	1	12
>5.91	0	0	12	0	12
Total	13	6	21	8	48

selection. Subsequently, the clustering in Experiment 1 was conducted and the functionality of the cluster groupings were compared in the *in vitro* system.

The distribution of the samples included in Experiment 2 across the *longissimus lumborum* clusters is presented in Table 6. Clusters were generally consistent with pH, but some samples with normal pH were included in the High pH cluster. System pH decline data were analyzed by ANOVA with mean comparisons for significant effects. Cluster and temperature decline rate interacted ($P < 0.001$) to affect pH decline in the *in vitro* system (Figure 5). Additionally, the pH decline rate for each cluster and temperature decline rate combination was estimated with an exponential decay function. Under the faster temperature decline, pH decline was slower and less extensive in the Soluble fraction causing the highest system pH values ($P < 0.05$) at 3, 6, and 24 h. The rate estimated by the exponential decay function was somewhat misleading for the Soluble cluster at the faster temperature decline rate. From the plot, it is evident that the decline in pH between 0 and 3 h in samples from the Soluble cluster was similar to the other clusters and that the final system pH for samples in this cluster was higher than for the other clusters (Figure 5). Because the final pH of the Soluble cluster was higher than the other clusters, the time required to reach the final pH was less in the Soluble cluster than for the other clusters. Thus, the rate to reach the final pH was estimated to be higher in the Soluble cluster than the other clusters even though pH decline was less extensive in this cluster.

When incubated with the faster temperature decline rate, system pH decline was more rapid in the High pH and Glycolytic clusters than in the Chaperone and Soluble clusters. Thus, system pH was lower ($P < 0.05$) in the High pH and Glycolytic clusters than the Soluble and Chaperone clusters at 3 and 6 h of incubation. The Chaperone cluster had intermediate pH values at 6 h of incubation but was similar in pH to the High pH and Glycolytic clusters at 24 h. Under the slower temperature decline, the Soluble cluster had the highest rate of pH decline and the lowest ($P < 0.05$) pH values after 3 h, while the Glycolytic and Chaperone clusters had the highest pH at 3 h of incubation. The Glycolytic and Chaperone clusters had higher ($P < 0.05$) pH values than the Soluble and High pH values at 6 h of incubation.

Glucose concentration was least ($P < 0.05$) in samples from the High pH cluster at the beginning of the

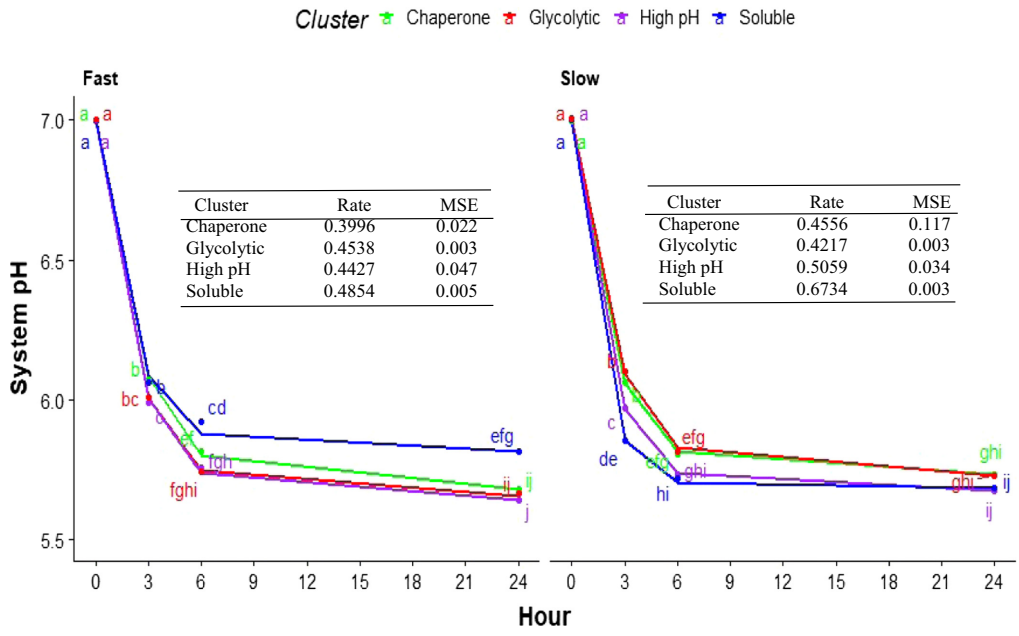

Figure 5. Least-squares means for system pH of *longissimus lumborum* muscles from cluster groupings based on metabolic traits incubated an *in vitro* system mimicking two different temperature declines rates. [a–j]Least-squares means lacking a common superscript differ ($P < 0.05$). Tabular data are the rate (α) from the exponential decay curve and the mean square error for α of each cluster under each temperature decline rate.

incubation period (Figure 6). Glucose concentration increased in all clusters with increased incubation time. However, glucose did not differ across *longissimus lumborum* clusters for the remaining time points sampled during the incubation period.

Glucose-6-phoshate increased ($P < 0.05$) in all clusters during incubation, particularly during the first 6 h (Figure 7). The High pH and Soluble clusters had higher ($P < 0.05$) glucose-6-phosphate levels at 3, 6, and 24 h of incubation than the Glycolytic and Chaperone clusters. After 24 h of incubation, the Chaperone cluster had glucose-6-phosphate concentrations similar to those detected in the High pH and Soluble clusters after 3 h. The Glycolytic cluster had lower glucose-6-phosphate concentrations than all the other clusters at 3, 6, and 24 h of incubation.

Lactate accumulated in the system with increased incubation time in all clusters during the first 6 h, and in the Chaperone cluster between 6 h and 24 h of incubation (Figure 8). System lactate was greater ($P < 0.05$) in the chaperone cluster than in samples from the High pH cluster at 3 h of incubation. Clusters did not differ in lactate at 6 h. At 24 h of incubation, samples from the Chaperone cluster had greater ($P < 0.05$) lactate content than the samples from the High pH and Soluble clusters.

The least-squares means for system glucose-6-phosphate concentration of *longissimus lumborum* samples incubated in an *in vitro* system with two different temperature decline rates are presented in Figure 9. Slower temperature decline resulted in greater ($P < 0.05$) glucose-6-phosphate levels at 6 and 24 h compared to the faster decline (Figure 5). Faster temperature decline resulted in greater ($P < 0.05$) lactate levels at 24 h of incubation compared to the slower decline (Figure 10).

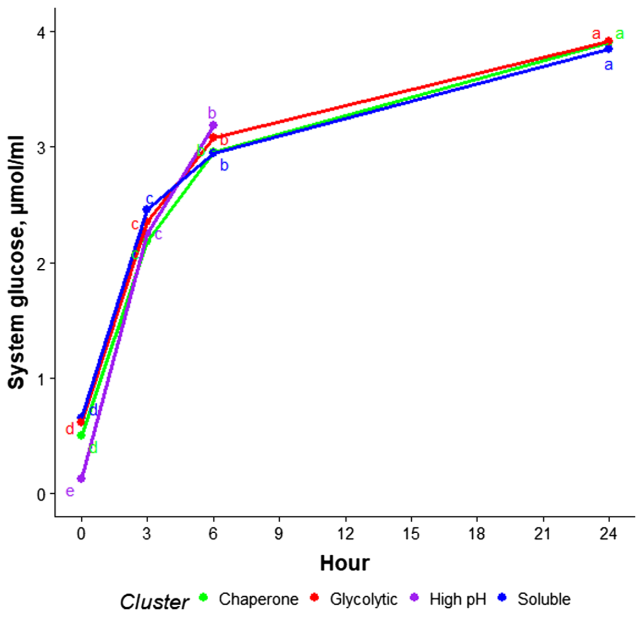

Figure 6. Least-squares means for system glucose of *longissimus lumborum* muscles from cluster groupings based on metabolic traits incubated in an *in vitro* system. [a–e]Least-squares means lacking a common superscript differ ($P < 0.05$).

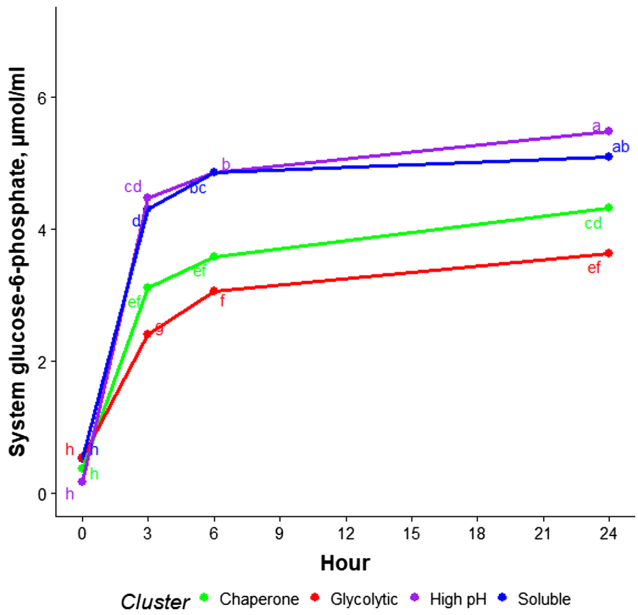

Figure 7. Least-squares means for system glucose-6-phosphate of *longissimus lumborum* muscles from cluster groupings based on metabolic traits incubated in an *in vitro* system. [a–h]Least-squares means lacking a common superscript differ ($P < 0.05$).

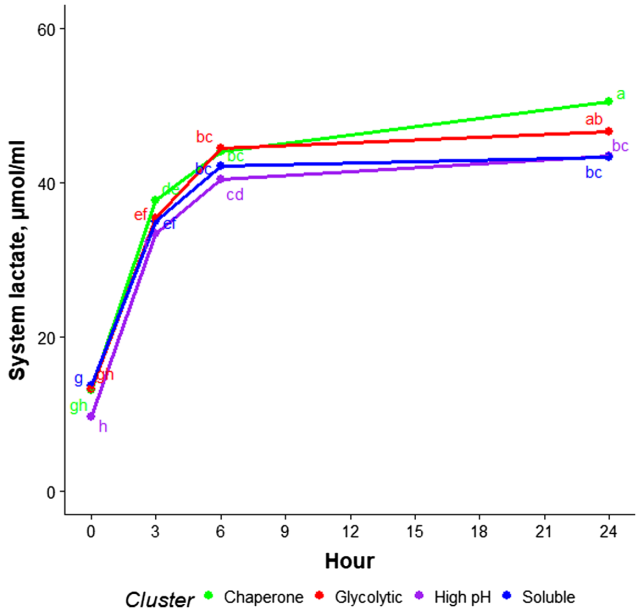

Figure 8. Least-squares means for system lactate of *longissimus lumborum* muscles from cluster groupings based on metabolic traits incubated in an *in vitro* system. [a–h]Least-squares means lacking a common superscript differ ($P < 0.05$).

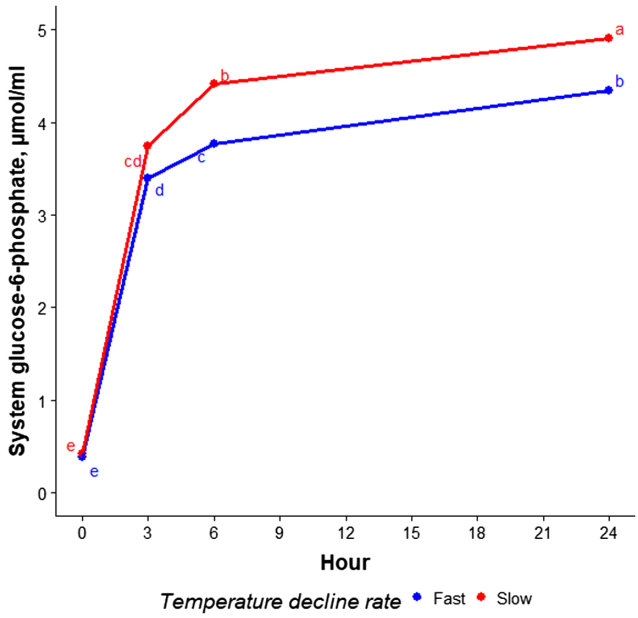

Figure 9. Least-squares means for system glucose-6-phosphate of *longissimus lumborum* muscles incubated in an *in vitro* system mimicking two different temperature decline rates. [a–e]Least-squares means lacking a common superscript differ ($P < 0.05$).

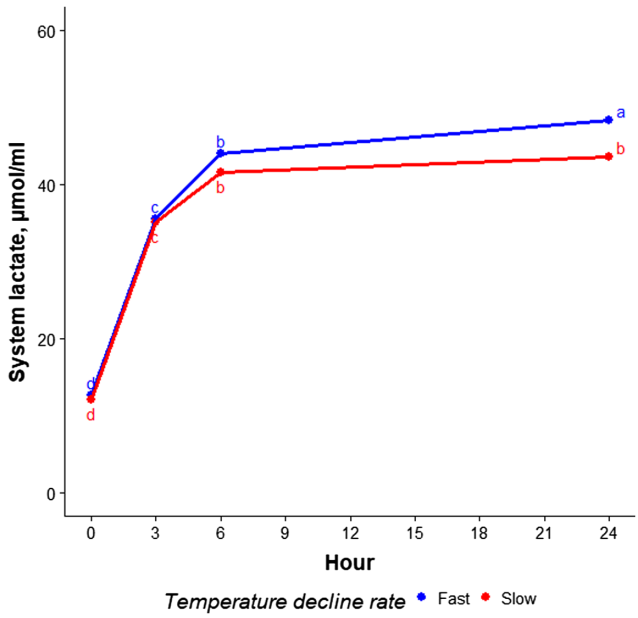

Figure 10. Least-squares means for system lactate of *longissimus lumborum* muscles incubated in an *in vitro* system mimicking two different temperature decline rates. [a–d]Least-squares means lacking a common superscript differ ($P < 0.05$).

The clustering employed in the present experiment segmented carcasses based on metabolic profile. Many of the traits included in the clustering were oxidative and not directly related to the glycolytic pathway. Still, we questioned whether the clusters would differ in the functionality of the glycolytic machinery. The *in vitro* system described by Scopes (1974) offered the opportunity to conduct this evaluation. Additionally, chilling conditions vary in commercial processing facilities and with variation in carcass size and fatness, so we questioned whether differing chilling rates would affect the efficiency of the glycolytic machinery. Thus, rather than incubating samples at a constant temperature, we simulated two different temperature decline rates during the incubation period.

The interaction between metabolic cluster and temperature decline rate to affect system pH decline indicates that, not only did the clusters differ in the function of the glycolytic machinery, but those differences also manifested differently at the two temperature decline rates. The largest difference between the two temperature decline rates was observed in the Soluble cluster. Under the slower temperature decline, samples in this cluster had the greatest rate of pH decline, resulting in lower system pH than the other clusters at 3 and 6 h of incubation. Under the faster temperature decline, samples from the Soluble cluster had a faster rate of pH decline than the other clusters, but also had less extensive pH decline than the other clusters and thus had higher system pH values at 6 and 24 h of incubation than the other clusters. Samples from the Soluble cluster had a much greater rate of pH decline under the slower temperature decline than under the faster temperature decline. The reason for this differential response to temperature decline is not clear. Relative to the other clusters, the Soluble cluster had the greatest protein solubility, greatest mitochondrial protein abundance, the greatest malate concentration, and lowest abundance of carbonyls on mitochondrial proteins and was intermediate in relation to the other clusters in respect to glycolytic metabolites. Mitochondrial protein has been shown to increase glycolytic flux (Matarneh et al., 2017), which may help explain the more rapid pH decline at the slower chilling rate. However, this is not consistent with the less extensive pH decline under the faster temperature decline rate. Perhaps one or more glycolytic enzyme is more susceptible to deactivation in muscles from the Soluble cluster. For example, phosphofructokinase catalyzes a key regulatory step of glycolysis and is deactivated by decreased muscle pH (England et al., 2014; Rhoades et al., 2005). England et al. (2014) suggested that a high rate of glycolysis would allow greater flux, and consequently a lower muscle pH, through phosphofructokinase before its inactivation by pH. The cluster differences in system glucose-6-phosphate concentrations were larger than the differences observed for other metabolites. The Glycolytic cluster had

the lowest accumulation of glucose-6-phosphate during the incubation period. The Chaperone cluster accumulated less glucose-6-phosphate in the *in vitro* system than the High pH and Soluble clusters. These differences did not reflect the differences in muscle concentrations of glucose-6-phosphate across clusters.

It is important to note that, *in situ*, multiple metabolic systems contribute to meeting energy demands by the muscle (Scheffler, 2024). These other pathways maintain functionality in postmortem muscle, particularly in the early postmortem period (England et al., 2018). Although mitochondrial function can affect pH decline and metabolite accumulation in this *in vitro* system (Scheffler et al., 2015), samples in the present experiment had been frozen and stored for an extended period. Thus, mitochondria were uncoupled and likely had no impact on glycolysis in the system in the present experiment. However, as noted earlier, mitochondrial protein can increase glycolytic flux (Matarneh et al., 2017). Hexokinase can bind to the mitochondrial membrane, which increases its activity in phosphorylating glucose (Wasserman, 2022). Cluster differences in glucose-6-phosphate may also indicate differences in the ability to generate energy via other pathways in the live animal. Glucose-6-phosphate can enter the pentose phosphate pathway, glycogen synthesis, *de novo* lipogenesis, and the hexosamine pathway (Rajas et al., 2019).

Conclusion

Deriving clusters from several metabolic traits was more effective in classifying muscles according to muscle metabolism than creating categories from muscle pH. Differences in muscle metabolism that were not explained by ultimate muscle pH existed in both *longissimus lumborum* and *gluteus medius* muscles. Metabolic traits differed between *gluteus medius* and *longissimus lumborum* muscles. However, similar relationships existed among metabolic traits in both muscles. Variation in the function of the glycolytic enzyme system was related to variation in metabolic status of postmortem muscle and can be differentially impacted by chilling rate. This may have profound implications for the development of meat quality traits during chilling and highlight a need to manage carcass chilling.

Acknowledgments

Mention of trade names or commercial products in this publication is solely for the purpose of providing specific information and does not imply recommendation or endorsement by the U.S. Department of Agriculture. The authors are grateful to Megan Landes-Murphy, Kristen Ostdiek, and Casey Trambly of the U.S. Meat Animal Research Center for their assistance in the execution of this experiment and to Jody Gallagher of the U.S. Meat Animal Research Center for her secretarial assistance. USDA is an equal opportunity provider and employer.

Author Contribution

D.A. King contributed to conceptualization, data curation, methodology, data analysis, writing, and original draft preparation. S.D. Shackelford contributed to methodology, data curation, and editing. D. Nonneman contributed to methodology and editing. T.S. Katz contributed to data analysis and editng. T.L. Wheeler contributed to methodology and editing.

Literature Cited

Apaoblaza, A., S. D. Gerrard, S. K. Matarneh, J. C. Wicks, L. Kirkpatrick, E. M. England, T. L. Scheffler, S. K. Duckett, H. Shi, S. L. Silva, A. L. Grant, and D. E. Gerrard. 2020. Muscle from grass- and grain-fed cattle differs energetically. Meat Sci. 161:107996. https://doi.org/10.1016/j.meatsci.2019.107996

Bendall, J. R. (Editor). 1973. Postmortem changes in muscle. In: Academic Press, New York, NY.

Bergmeyer, H. U. 1974. Methods of enzymatic analysis. 2nd edition. Elsevier.

Carlson, K. B., K. J. Prusa, C. A. Fedler, E. M. Steadham, E. Huff-Lonergan, and S. M. Lonergan. 2017. Proteomic features linked to tenderness of aged pork loins. J. Anim. Sci. 95:2533–2546. https://doi.org/10.2527/jas.2016.1122

Cawthon, D., K. Beers, and W. G. Bottje. 2001. Electron transport chain defect and inefficient respiration may underlie pulmonary hypertension syndrome (ascites)-associated mitochondrial dysfunction in broilers. Poultry Sci. 80:474–484. https://doi.org/10.1093/ps/80.4.474

Eilers, J. D., J. D. Tatum, J. B. Morgan, and G. C. Smith. 1996. Modification of early-postmortem muscle pH and use of postmortem aging to improve beef tenderness. J. Anim. Sci. 74:790–798.

England, E. M., S. K. Matarneh, R. M. Mitacek, A. Abraham, R. Ramanathan, J. C. Wicks, H. Shi, T. L. Scheffler, E. M. Oliver, E. T. Helm, and D. E. Gerrard. 2018. Presence of oxygen and mitochondria in skeletal muscle early postmortem. Meat Sci. 139:97–106. https://doi.org/10.1016/j.meatsci.2017.12.008

England, E. M., S. K. Matarneh, E. M. Oliver, A. Apaoblaza, T. L. Scheffler, H. Shi, and D. E. Gerrard. 2016. Excess glycogen does not resolve high ultimate pH of oxidative muscle. Meat Sci. 114:95–102. https://doi.org/10.1016/j.meatsci.2015.10.010

England, E. M., S. K. Matarneh, T. L. Scheffler, C. Wachet, and D. E. Gerrard. 2014. pH inactivation of phosphofructokinase

arrests postmortem glycolysis. Meat Sci. 98:850–857. https://doi.org/10.1016/j.meatsci.2014.07.019

English, A. R., K. M. Wills, B. N. Harsh, G. G. Mafi, D. L. VanOverbeke, and R. Ramanathan. 2016. Effects of aging on the fundamental color chemistry of dark-cutting beef. J. Anim. Sci. 94:4040–4048. https://doi.org/10.2527/jas.2016-0561

Galili, T. 2015. dendextend: an R package for visualizing, adjusting and comparing trees of hierarchical clustering. Bioinformatics 31:3718–3720. https://doi.org/10.1093/bioinformatics/btv428

Hammelman, J. E., B. C. Bowker, A. L. Grant, J. C. Forrest, A. P. Schinckel, and D. E. Gerrard. 2003. Early postmortem electrical stimulation simulates PSE pork development. Meat Sci. 63:69–77. https://doi.org/10.1016/s0309-1740(02)00057-8

Harrel, F. E., Jr., and C. Dupont. 2020. Hmisc: Harrel Miscellaneous. https://CRAN.R-project.org/package=Hmisc

Hunt, M. C., and H. B. Hedrick. 1977. Profile of fiber types and related properties of five bovine muscles. J. Food Sci. 42:513–517. https://doi.org/10.1111/j.1365-2621.1977.tb01535.x

Iqbal, M., N. R. Pumford, Z. X. Tang, K. Lassiter, C. Ojano-Dirain, T. Wing, M. Cooper, and W. Bottje. 2005. Compromised liver mitochondrial function and complex activity in low feed efficient broilers are associated with higher oxidative stress and differential protein expression. Poultry Sci. 84:933–941. https://doi.org/10.1093/ps/84.6.933

Jeremiah, L. E., A. K. W. Tong, and L. L. Gibson. 1991. The usefulness of muscle color and pH for segregating beef carcasses into tenderness groups. Meat Sci. 30:97–114. https://doi.org/10.1016/0309-1740(91)90001-7

Johnson, L. G., E. M. Steadham, E. J. Huff-Lonergan, and S. M. Lonergan. 2021. Partial purification of peroxiredoxin-2 from porcine skeletal muscle. Meat Muscle Biol. 5:29, 1–9. https://doi.org/10.22175/mmb.12408

Jones, B. K., and J. D. Tatum. 1994. Predictors of beef tenderness among carcasses produced under commercial conditions. J. Anim. Sci. 72:1492–1501. https://doi.org/10.2527/1994.7261492x

Kassambara, A., and F. Mundt. 2020. factoextra: Extract and visualize the results of multivariate data analyses, R package version 1.0.7. https://CRAN.R-project.org/package=factoextra

King, D. A., M. C. Hunt, S. Barbut, J. R. Claus, D. P. Cornforth, P. Joseph, Y. H. B. Kim, G. Lindahl, R. A. Mancini, M. N. Nair, K. J. Merok, A. Milkowski, A. Mohan, F. Pohlman, R. Ramanathan, C. R. Raines, M. Seyfert, O. Sørheim, S. P. Suman, and M. Weber. 2023. American Meat Science Association Guidelines for Meat Color Measurement. Meat Muscle Biol. 6:12473, 1–81. https://doi.org/10.22175/mmb.12473

King, D. A., R. K. Miller, R. O. McKeith, A. L. Grayson, S. D. Shackelford, K. B. Gehring, J. W. Savell, and T. L. Wheeler. 2024. Multivariate examination of metabolic contributions to beef longissimus lumborum flavor. Meat Muscle Biol. 8:1–14. https://doi.org/10.22175/mmb.17055

Kirkpatrick, L. T., J. F. M. Gómez, M. Beline, C. N. Yen, J. S. Bodmer, J. C. Wicks, T. H. Shi, S. L. Silva, J. L. Aalhus, D. A. King, and D. E. Gerrard. 2023. Muscle of dark and normal beef differs metabolically. Meat Sci. 206:109344. https://doi.org/10.1016/j.meatsci.2023.109344

Kiyimba, F., S. D. Hartson, J. Rogers, D. L. VanOverbeke, G. G. Mafi, and R. Ramanathan. 2021. Changes in glycolytic and mitochondrial protein profiles regulates postmortem muscle acidification and oxygen consumption in dark-cutting beef. J. Proteomics 232:104016. https://doi.org/10.1016/j.jprot.2020.104016

Lanari, M. C., and R. G. Cassens. 1991. Mitochondrial activity and beef muscle color stability. J. Food Sci. 56:1476–1479. https://doi.org/10.1111/j.1365-2621.1991.tb08619.x

Le, S., J. Josse, and F. Husson. 2008. FactoMineR: An R package for multivariate analysis. J. Stat. Softw. 25:1–18. https://doi.org/10.18637/jss.v025.i01

Matarneh, S. K., E. M. England, T. L. Scheffler, C.-N. Yen, J. C. Wicks, H. Shi, and D. E. Gerrard. 2017. A mitochondrial protein increases glycolytic flux. Meat Sci. 133:119–125. https://doi.org/10.1016/j.meatsci.2017.06.007

Mayer, T. R., S. E. Borders, T. E. Schwartz, K. B. Gehring, D. B. Griffin, C. R. Kerth, K. E. Belk, J. A. Scanga, M. N. Nair, M. M. Pfeiffer, G. G. Mafi, K. M. Harr, T. E. Lawrence, T. C. Tennant, L. W. Lucherk, T. G. O'Quinn, E. S. Beyer, P. D. Bass, L. G. Garcia, B. M. Bohrer, J. A. Pempek, A. J. Garmyn, R. J. Maddock, C C. Carr, T. D. Pringle, T. L. Scheffler, J. M. Scheffler, A. M. Stelzleni, J. M. Gonzalez, K. R. Underwood, B. N. Harsh, C. M. Waters, and J. W. Savell. 2024. National Beef Quality Audit—2022: In-plant assessments of quality and yield determining carcass characteristics of fed steers and heifers. Translational Animal Science 8:txae098. https://doi.org/10.1093/tas/txae098

McKeith, R. O., D. A. King, A. L. Grayson, S. D. Shackelford, K. B. Gehring, J. W. Savell, and T. L. Wheeler. 2016. Mitochondrial abundance and efficiency contribute to lean color of dark cutting beef. Meat Sci. 116:165–173. https://doi.org/10.1016/j.meatsci.2016.01.016

McKenna, D. R., P. D. Mies, B. E. Baird, K. D. Pfeiffer, J. W. Ellebracht, and J. W. Savell. 2005. Biochemical and physical factors affecting discoloration characteristics of 19 bovine muscles. Meat Sci. 70:665–682. https://doi.org/10.1016/j.meatsci.2005.02.016

Mitacek, R. M., Y. Ke, J. E. Prenni, R. Jadeja, D. L. VanOverbeke, G. G. Mafi, and R. Ramanathan. 2019. Mitochondrial degeneration, depletion of NADH, and oxidative stress decrease color stability of wet-aged beef longissimus steaks. J. Food Sci. 84:38–50. https://doi.org/10.1111/1750-3841.14396

Monin, G., and P. Sellier. 1985. Pork of low technological quality with a normal rate of muscle pH in the immediate post-mortem perdiod: the case of the Hampshire breed. Meat Sci. 13:49–63.

Picard, B., C. Barboiron, D. Chadeyron, and C. Jurie. 2011. Protocol for high-resolution electrophoresis separation of myosin heavy chain isoforms in bovine skeletal muscle. Electrophoresis 32:1804–1806. https://doi.org/10.1002/elps.201100118

Picard, B., M. Gagaoua, D. Micol, I. Cassar-Malek, J.-F. Hocquette, and C. E. M. Terlouw. 2014. Inverse relationships between biomarkers and beef tenderness according to contractile and metabolic properties of the muscle. J. Agr. Food Chem. 62:9808–9818. https://doi.org/10.1021/jf501528s

R Development Core Team, 2008, R: A language and environment for statistical computing., URL http://www.R-project.org.

Rajas, F., A. Gautier-Stein, and G. Mithieux. 2019. Glucose-6 phosphate, a central hub for liver carbohydrate metabolism. Metabolites 9:282. https://doi.org/10.3390/metabo9120282

Ramanathan, R., F. Kiyimba, J. Gonzalez, G. Mafi, and U. DeSilva. 2020. Impact of up- and downregulation of metabolites and mitochondrial content on ph and color of the longissimus muscle from normal-ph and dark-cutting beef. J. Agr. Food Chem. 68:7194–7203. https://doi.org/10.1021/acs.jafc.0c01884

Ramanathan, R., M. N. Nair, M. C. Hunt, and S. P. Suman. 2019. Mitochondrial functionality and beef colour: A review of recent research. S. Afr. J. Anim. Sci. 49. https://doi.org/10.4314/sajas.v49i1.2

Ramos, P. M., M. R. Pedrão, L. C. Bell, and T. L. Scheffler. 2021. Early postmortem metabolism and protease activation in fast glycolytic and slow oxidative bovine muscles. Meat Muscle Biol. 5:44, 1–10. https://doi.org/10.22175/mmb.12977

Ramos, P. M., S. A. Wright, E. F. Delgado, E. van Santen, D. D. Johnson, J. M. Scheffler, M. A. Elzo, C. C. Carr, and T. L. Scheffler. 2020. Resistance to pH decline and slower calpain-1 autolysis are associated with higher energy availability early postmortem in Bos taurus indicus cattle. Meat Sci. 159:107925. https://doi.org/10.1016/j.meatsci.2019.107925

Reznick, A. Z., and L. Packer. 1994. Oxidative damage to proteins: spectrophotometric method for carbonyl assay. Method. Enzymol. 233:357–363. https://doi.org/10.1016/s0076-6879(94)33041-7

Rhoades, R. D., D. A. King, B. E. Jenschke, J. M. Behrends, T. S. Hively, and S. B. Smith. 2005. Postmortem regulation of glycolysis by 6-phosphofructokinase in bovine M. Sternocephalicus pars mandibularis. Meat Sci. 70:621–626. https://doi.org/10.1016/j.meatsci.2005.01.024

Rowe, L. J., K. R. Maddock, S. M. Lonergan, and E. Huff-Lonergan. 2004. Influence of early postmortem protein oxidation on beef quality. J. Anim. Sci. 82:785–793. https://doi.org/10.2527/2004.823785x

Scheffler, T. L. 2024. Resilience in life and death: Metabolism and proteolysis in *Bos indicus* muscle and meat. Meat Sci. 218:109622. https://doi.org/10.1016/j.meatsci.2024.109622

Scheffler, T. L., S. K. Matarneh, E. M. England, and D. E. Gerrard. 2015. Mitochondria influence postmortem metabolism and pH in an in vitro model. Meat Sci. 110:118–125. https://doi.org/10.1016/j.meatsci.2015.07.007

Schmittgen, T. D., and K. J. Livak. 2008. Analyzing real-time PCR data by the comparative CT method. Nat. Protoc. 3:1101–1108. https://doi.org/10.1038/nprot.2008.73

Scopes, R. K. 1974. Studies with a reconstituted muscle glycolytic system. The rate and extent of glycolysis in simulated post-mortem conditions. Biochem. J. 142:79–86. https://doi.org/10.1042/bj1420079

USDA. 2014. Institutional Meat Purchase Specifications Fresh Beef Series 100. https://www.ams.usda.gov/sites/default/files/media/IMPS_100_Fresh_Beef%5B1%5D.pdf. (Accessed 3 May 2018).

Wang, C., M. J. Taylor, C. D. Stafford, D. S. Dang, S. K. Matarneh, D. E. Gerrard, and J. Tan. 2024. Analysis of phosphofructokinase-1 activity as affected by pH and ATP concentration. Sci. Rep.-UK 14:21192. https://doi.org/10.1038/s41598-024-72028-4

Wasserman, D. H. 2022. Insulin, muscle glucose uptake, and hexokinase: revisiting the road not taken. Physiology 37:115–127. https://doi.org/10.1152/physiol.00034.2021

Wright, S. A., P. Ramos, D. D. Johnson, J. M. Scheffler, M. A. Elzo, R. G. Mateescu, A. L. Bass, C. C. Carr, and T. L. Scheffler. 2018. Brahman genetics influence muscle fiber properties, protein degradation, and tenderness in an Angus-Brahman multibreed herd. Meat Sci. 135:84–93. https://doi.org/10.1016/j.meatsci.2017.09.006

Wulf, D. M., R. S. Emnett, J. M. Leheska, and S. J. Moeller. 2002. Relationships among glycolytic potential, dark cutting (dark, firm, and dry) beef, and cooked beef palatability. J. Anim. Sci. 80:1895–1903. https://doi.org/10.2527/2002.8071895x